coatings

MDPI

Article

Study on Macroscopic Mechanical Properties and Microscopic Mechanism of Drilling Cuttings Solidified by Alkali-Activated Furnace Ash

Achen Qi [1], Pei Wang [2], Yuanjie Zhu [3], Wei Liu [4], Jianghua Jia [5], Zixuan Wang [5], Wenjun Hu [5,*] and Yumei Liu [5,*]

[1] Heavy Oil Development Company of PetroChina Xinjiang Oilfield Company, Karamay 834000, China; qiachen@petrochina.com.cn
[2] Fengcheng Oilfield Operation Area, PetroChina Xinjiang Oilfield Company, Karamay 834000, China; fcwp@petrochina.com.cn
[3] Production and Operation Department, PetroChina Xinjiang Oilfield Company, Karamay 834000, China; yqcyzyj88@petrochina.com.cn
[4] Oil Production Technology Research Institute, PetroChina Xinjiang Oilfield Company, Karamay 834000, China; lw688@petrochina.com.cn
[5] School of Transportation Engineering, Shandong Jianzhu University, Jinan 250101, China; huayv20010927@163.com (J.J.); 19863678503@163.com (Z.W.)
* Correspondence: huwenjun@sdjzu.edu.cn (W.H.); liuyumei22@sdjzu.edu.cn (Y.L.)

Highlights

What are the main findings?

- NaOH activator yields optimal mechanical properties with 4.81 MPa compressive strength at 28 days.
- Hydration products primarily consist of C-(N)-A-S-H and C-S-H gels under a high alkaline environment.
- Activator type directly regulates hierarchical differences in mechanical properties through hydration kinetics.

What are the implications of the main findings?

- Provide a technical pathway for high-value utilization of oilfield solid waste materials.
- Offer the theoretical basis for engineering application of solid waste-based cementitious materials.
- Promote a green and low-carbon transformation of transportation infrastructure.

Abstract

To promote the resource utilization of oilfield solid waste and facilitate the green and low-carbon transformation of transportation infrastructure, this study employed drilling cuttings from the Maye area of the Xinjiang oilfield and coal-fired furnace ash as primary raw materials. NaOH, $Na_2O{\cdot}nSiO_2$, and $Ca(OH)_2$ were used as alkali activators to prepare alkali-activated solidification materials for oilfield road base applications. The optimal curing system identified in this study (4 wt.% NaOH + 20 wt.% furnace ash) falls within the commonly reported dosage ranges for alkali-activated solid-waste materials, where NaOH contents are typically 3%–8% and furnace ash contents 15%–30%. Considering the distinct chemical characteristics of the Xinjiang oilfield solid wastes, a targeted optimization strategy was adopted to achieve a balance between mechanical performance and economic feasibility. Based on mix-proportion experiments, macroscopic mechanical properties were evaluated. In combination with X-ray diffraction (XRD), laser particle size analysis, simultaneous thermal analysis (TG–DSC), and scanning electron microscopy coupled with energy-dispersive spectroscopy (SEM–EDS), the influence of activator type on both

Academic Editor: Paolo Castaldo

Received: 22 January 2026
Revised: 10 February 2026
Accepted: 18 February 2026
Published: 23 February 2026

mechanical performance and microstructural evolution was systematically investigated. The results indicate that the system containing 4 wt.% NaOH + 20 wt.% furnace ash exhibits the best overall performance, achieving a 28-day compressive strength of 4.81 MPa and a splitting tensile strength of 0.41 MPa, which are significantly higher than those of the $Na_2O{\cdot}nSiO_2$ system (3 wt.% $Na_2O{\cdot}nSiO_2$ + 20 wt.% furnace ash) and the $Ca(OH)_2$ system (4 wt.% $Ca(OH)_2$ + 15 wt.% furnace ash). The primary hydration products were identified as C-(N)-A-S-H and C-S-H gels. The type of alkali activator plays a decisive role in regulating hydration reaction kinetics and the spatial distribution of Ca and Si elements, thereby governing the hierarchical differences in macroscopic mechanical properties. In particular, NaOH generates a highly alkaline environment that promotes the dissolution of active Si/Al components in both drilling cuttings and furnace ash, enhances gel polymerization, and results in a denser microstructure. This study provides theoretical and technical support for the high-value utilization of oilfield solid wastes in highway base engineering.

Keywords: oilfield drilling cuttings; coal-fired furnace ash; alkali-activated curing material; mechanical properties; microscopic characteristics

1. Introduction

With the continuous development of China's petroleum industry, oilfield exploration and development activities are becoming more and more frequent. The long-term accumulation of multi-source solid waste generated in the process of oilfield exploration and development, gathering and transportation, and supporting energy security, especially the increasing production of solid waste materials such as drilling cuttings and coal-fired furnace ash, have become some of the important problems restricting the ecological environment safety and sustainable utilization of resources in oilfield areas [1]. At present, the disposal methods of drilling cuttings and coal-fired furnace ash in oilfields are still mainly stacking or simple landfill, which occupy a large amount of land resources. Moreover, heavy metals, soluble salts, and potential pollutants contained in solid waste are prone to migrate during long-term storage, posing a pollution risk to the soil and groundwater environment, and thus adversely affecting the regional ecosystem and the surrounding environmental safety of oil fields [2,3].

In the construction of transportation infrastructure, such as oil fields roads, the subgrade and pavement base have a great demand for materials and strong adaptability, which provides an important engineering carrier for the in situ resource utilization of oilfields' solid waste. The synergistic application of drilling cuttings, coal-fired furnace ash, and other oilfield solid wastes in road engineering not only helps to alleviate the environmental pressure caused by the centralized storage of solid wastes but also significantly reduces the consumption of non-renewable resources such as cement, lime, and natural aggregates. It is of great practical significance to promote the transformation of oilfield infrastructure construction in a green, low-carbon, and recycling direction. In this context, alkali-activated cementitious materials (AACM) have become a research hotspot in the field of solid waste resource utilization because they can react with silicon-containing aluminum solid waste by means of alkaline activators to produce hydration products with cementitious properties [4,5]. Compared with traditional cement, the alkali-activated cementitious material does not need to be calcined at a high temperature during the preparation process, and the carbon emission is reduced by about 80%. It has the advantages of solid waste resource utilization and good engineering application potential [6–8].

In recent years, domestic and foreign scholars have carried out a lot of research on alkali-activated cementitious materials around different solid waste systems. Studies have shown that a variety of solid waste materials can form a stable cementitious structure under suitable alkali activation conditions for road engineering construction. Gao et al. [9] used red mud, carbide slag, and slag as raw materials to prepare all-solid waste alkali-activated cementitious materials, and used them as binders to develop stable red sand soil (FSCMS) semi-rigid base materials. Through the research on the road performance and microscopic characteristics of FSCMS, it is shown that when the binder content is 20%, the 7-day unconfined compressive strength of FSCMS is 2.6 MPa, and the water stability coefficient is 0.67, which meets the requirements of high-grade highways. The C-A-S-H gel generated by the alkali-activated reaction has pore filling and chemical cementation, which can significantly improve the mechanical properties of the base material. Jing et al. [10] used spontaneous combustion coal gangue as the main raw material to prepare ternary alkali-activated cementitious materials with granulated blast furnace slag and fly ash. Based on compressive strength and fluidity, the ratio was optimized, and a variety of test methods were used to explore the effect of spontaneous combustion coal gangue content and alkali activator content on the macroscopic properties and microstructure evolution of the cementitious materials. Li et al. [11] prepared five kinds of alkali-activated slag pastes with different Ca/Si ratios, and studied the changes in fluidity, setting time, and compressive strength with modulus (M), Na mass fraction (Nc), and Ca/Si ratio. Through X-ray diffraction (XRD), Fourier transform infrared spectroscopy (FT-IR), and energy dispersive spectroscopy scanning electron microscopy (SEM-EDS), the control mechanism of microstructure difference in the alkali-activated slag system on the development of macroscopic properties was clarified. Li et al. [12] studied the structural characteristics, hydration mechanism, and cementitious structure of XSG (a kind of composite functional curing agent specially designed for the solidification of waste drilling fluid, whose main components are alkaline regulating components, gelation accelerators and adsorbents) curing agent, and clarified the principle of curing waste drilling fluid. Yang et al. [13] studied the composition of XSG curing agent and the effect of different formulations, and verified its applicability to multi-system waste drilling fluid.

Han B et al. [14] systematically investigated the fluidity, autogenous shrinkage, and mechanical properties of alkali-activated slag grouting materials. It was found that the introduction of an appropriate amount of metakaolin was helpful to optimize the comprehensive properties of alkali-activated slag grouting materials. Song et al. [15] used a large amount of steel slag as the main raw material, and used alkali activator to stimulate the cementitious properties of steel slag. At the same time, silica fume and quartz powder were introduced to regulate the silicon source and optimize the ratio of cementitious materials. The effects of different activator content and silicon source on the mechanical properties and strength evolution mechanism of steel slag-based alkali-activated cementitious materials were investigated. Fu et al. [16] tried to use alkali activation technology to solidify drilling cuttings containing high organic matter, and studied the solidification technology of drilling cuttings. The results show that the mechanical properties and structural compactness of solidified materials can be effectively improved by regulating the silicon-calcium ratio and activator system, which provides a technical path for the engineering utilization of drilling cuttings in oilfields.

The existing research has fully confirmed the feasibility and advantages of alkali activation technology in the utilization of various solid waste resources. However, the research on the synergistic alkali activation curing system of oilfield drilling cuttings and coal-fired furnace ash is still limited. Especially under the action of different alkali activators, the synergistic effect of the two types of solid waste in the reaction process, the composition and

microstructure evolution mechanism of cementitious products are still lacking systematic understanding. Based on this, this study takes oilfield drilling cuttings and coal-fired furnace ash as the research object, constructs a synergistic curing system under different alkali activator conditions, and systematically studies its macroscopic mechanical properties and microscopic mechanism. The compressive strength and other mechanical properties of solidified drilling cuttings at different ages were tested by reasonably designing the key parameters, such as the compound ratio of furnace ash and drilling cuttings, the type and dosage of alkali activator. At the same time, combined with XRD, SEM-EDS, TG-DSC, laser particle size analysis, and other microscopic characterization methods, the phase composition, microstructure, and other characteristics of the gelled products are revealed, and the synergistic reaction mechanism of furnace ash and drilling cuttings in the alkali activation process is clarified. It provides a theoretical basis and technical support for the resource utilization of multi-source solid wastes in oilfields in engineering fields such as road semi-rigid bases.

2. Raw Materials

The drilling cuttings are taken from the Maye oil well in the Karamay oilfield, Xinjiang. The basic properties of the drilling cuttings are shown in Table 1, and the natural state at room temperature is shown in Figure 1a. Furnace ash is an industrial solid waste produced by coal-fired heating or power systems in oil fields. It is prepared by mechanical crushing after boiler slag removal, pretreatment, impurity removal, and drying. In order to clarify the phase composition of the furnace ash, the X-ray diffraction (XRD, Rigaku Corporation, Tokyo, Japan) test was carried out on the soil sample after grinding and passing through the 0.05 mm sieve. The scanning range was 5~80° and the scanning speed was 2°/min. The phase composition of the furnace ash is shown in Figure 2a. According to the analysis, the main components are quartz (SiO_2) and calcium oxide (CaO).

Table 1. Basic properties of drilling cuttings.

Maximum Dry Density (g/cm^3)	Optimum Moisture Content (%)	Cohesive Force (kPa)	Angle of Internal Friction (°)	Modulus of Resilience (MPa)	Modulus of Compression (MPa)
2.11	10.2	38.66	9	24.23	4.49

(**a**) (**b**)

Figure 1. Drilling cuttings and coal-fired furnace ash: (**a**) Drilling cuttings; (**b**) furnace ash.

To further characterize the chemical composition of the furnace ash, the oxide contents were quantitatively determined using X-ray fluorescence spectroscopy (XRF, Rigaku Corporation, Tokyo, Japan). As shown in Figure 2b, the predominant oxides are SiO_2 (29.5 wt.%) and CaO (26.3 wt.%), followed by Al_2O^3 (14.3 wt.%) and Fe_2O^3 (11.9 wt.%). Minor constituents include MgO (6.7 wt.%) and SO^3 (5.7 wt.%), along with trace amounts of TiO_2, Na_2O, K_2O, MnO, BaO, and SrO. The relatively high contents of SiO_2 and CaO are consistent with the XRD results, indicating that the furnace ash is rich in available silicon and calcium sources, which provide favorable conditions for subsequent alkali-activation reactions.

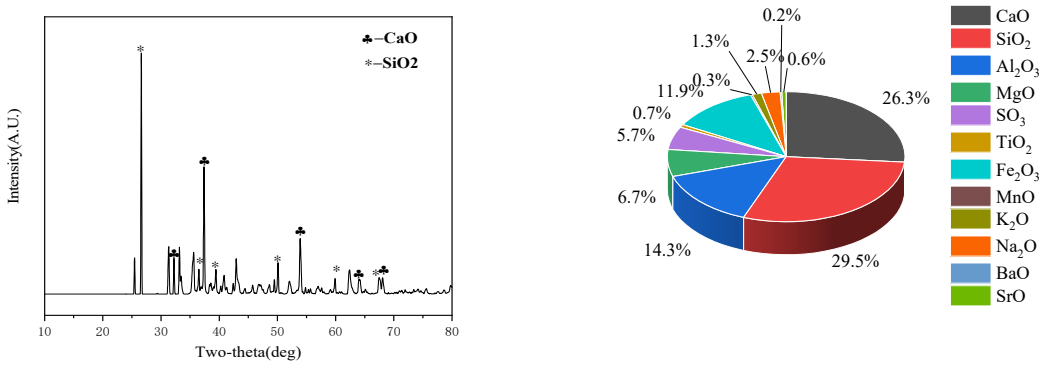

(**a**) (**b**)

Figure 2. XRD pattern and XRF oxide composition of the furnace ash: (**a**) XRD pattern; (**b**) XRF oxide composition of the furnace ash.

As shown in Table 2, $Na_2O{\cdot}nSiO_2$ with a modulus of 2.23, analytically pure NaOH with a purity of 96%, and analytically pure $Ca(OH)_2$ with a purity of ≥95% were selected as alkali activators. The three alkali activators are presented in Figure 3. The alkaline regulation systems adopted in this study are categorized into two types, which exhibit essential differences in both reaction mechanism and reaction rate: (1) Strong alkaline activators (NaOH, $Na_2O{\cdot}nSiO_2$): These agents can construct a strong alkaline environment with pH > 12.5, which rapidly dissolves the active Si/Al components in furnace ash and drilling cuttings, and initiates a rapid alkali-activated polymerization reaction to form C-(N)-A-S-H and C-S-H gels. (2) Calcium-based alkaline regulator ($Ca(OH)_2$): This agent only releases Ca^{2+} and maintains a mild alkaline environment with pH ≈ 11.5–12.0, which is insufficient to rapidly dissolve the active Si/Al components. Instead, it only promotes a slow pozzolanic reaction, whereby Ca^{2+} ions gradually combine with active Si species to form a small amount of C-S-H gel. Its action mechanism is thus significantly distinct from the rapid polymerization reaction induced by strong alkaline activators. For the solid waste of other oil fields, the content of main oxides (SiO_2, Al_2O_3, CaO) can be tested by XRF. The higher the content of active Si/Al, the lower the content of NaOH. When the CaO content is high, the principle of 'furnace ash ratio can be fine-tuned' is suitable for the optimal ratio. The results of this study can be used as a benchmark scheme for cross-field promotion.

Table 2. Basic properties of $Na_2O{\cdot}nSiO_2$.

Modulus($nSiO_2/nNa_2O$)	Transparency	SiO_2/%	Na_2O/%	Baume Degree/°Bé	Bulk Density/($t{\cdot}m^{-3}$)
2.23	85	≥29.50	≥14.00	50.0–51.0	1.526–1.543

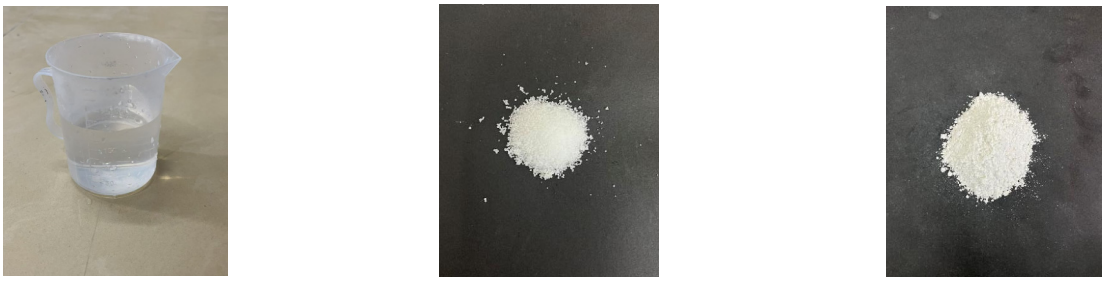

(**a**) (**b**) (**c**)

Figure 3. Three alkali activators: (**a**) $Na_2O{\cdot}nSiO_2$; (**b**) sodium hydroxide; (**c**) calcium hydroxide.

3. Test Methods

3.1. Mix Design

To determine the optimal combination of alkali activator type, activator dosage, and furnace ash content, a controlled variable experimental approach was adopted based on the key influencing parameters of alkali-activated solidified materials. The 7-day unconfined compressive strength was selected as the primary evaluation index for mix proportion optimization. The experimental factors and their corresponding levels are presented in Table 3. The optimal proportions for each alkali activator system were identified through a comparative analysis of the strength results under different dosage combinations.

Table 3. Orthogonal test factor level table.

No.	Activator Dosage (wt.%)	Furnace Ash Dosage (wt.%)
1	3	10
2	4	15
3	5	20
4	3	15
5	4	20
6	5	10
7	3	20
8	4	10
9	5	15

3.2. Mechanical Properties Test

According to the requirements of the "Test Specification for Inorganic Binder Stabilized Materials for Highway Engineering" (JTG 3441-2024) [17], a cylindrical specimen with a diameter-height ratio of 1:1 was used in this test. The specimen was formed under 2 MPa static pressure load for 30 s, and the dimensional tolerance of the specimen was controlled within ±1.0 mm after forming.

The specimens were cured in an HWHS-60B constant temperature and humidity curing chamber, with the temperature set at 20 °C ± 2 °C and the relative humidity maintained at no less than 95%. During the curing period, temperature and humidity were recorded at 8:00 and 20:00 daily; the actual measured temperature fluctuation range was 19.8 °C to 20.5 °C, and the relative humidity was stably maintained at 96% ± 1%. After curing to the designated age, the apparent density of specimens was determined via the drainage method in accordance with the JTG 3441-2024 [17]. The average apparent density of specimens cured for 7 days was 2.18 g/cm^3, and that for 28 days of curing was 2.24 g/cm^3.

Unconfined compressive strength tests were conducted on cylindrical specimens with dimensions of ∅100 mm × 100 mm using an LD-127 pavement strength tester, at a loading rate of 1 mm/min. Three replicate specimens were prepared for each test group, and the final test results were presented as the average value.

Splitting tensile strength test was carried out on the same specimen. The specimen was placed horizontally in the splitting fixture. The width of the clamp strip was 12.7 mm, the radius of the arc surface was 50 mm, and the loading rate was also 1 mm/min. The average value of the three specimens was evaluated.

In order to evaluate the dry–wet alternate resistance of the solidified body, the specimens after 28 days of standard curing were subjected to dry–wet cycle treatment according to the specification JTG 3441-2024 [17] and related durability test methods. The single

cycle consists of two stages: natural drying for 24 h and soaking in water at 20 ± 2 °C for 24 h. The specimens after 1,3,5,7 and 9 cycles were tested respectively, and three parallel specimens were set up in each group. The unconfined compressive strength test was carried out immediately after the end of the cycle, and the loading rate was 1 mm/min. The durability was evaluated by calculating the strength retention rate (the percentage of the strength after the dry–wet cycle to the strength of the standard curing specimen in the same period).

3.3. Microscopic Test

3.3.1. XRD Test

The solidified drilling cuttings specimens cured to the specified age were dried to constant weight in an oven at 50 °C (±2 °C), ground into powder, and tableted. The phase analysis of hydration products of different solidified drilling cuttings samples was carried out by the Smartlab SE XRD instrument. The scanning range was 5~80°, and the scanning speed was 2°/min. Jade 6.0 software was used for analysis. The XRD data were smoothed, and the background was deducted. Then, the database was used to identify each diffraction peak and identify the known phase.

3.3.2. Laser Particle Size Analysis Test

The solidified drilling cuttings were dried to constant weight and ground into powder. After passing through the 200-mesh sieve, the key indicators, such as the particle size distribution curve and the characteristic particle size parameters of the samples, were obtained by using the LS-609 laser particle size analyzer (Zhuhai OMEC Instruments Co., Ltd., Zhuhai, China). The particle size information of the particles in the concentrated area and the discrete area can be obtained intuitively through the test results. The cumulative distribution curve can reflect the proportion of fine particles.

3.3.3. TG-DSC Test

The solidified drilling cuttings were dried to constant weight and ground to powder by Rigaku TG/DTA 8122 thermogravimetric analyzer (Rigaku Corporation, Tokyo, Japan), and the hydration products were analyzed by synchronous thermal analysis. The test temperature was 30~800 °C, the heating rate was 10 °C/min, and the environment was nitrogen.

3.3.4. SEM-EDS Test

The solidified drilling cuttings were dried to constant weight and then crushed into blocks, with a length and width of more than 1 cm, for SEM-EDS testing. In this paper, the Gemini SEM 300, an SEM-EDS instrument (Carl Zeiss AG, Oberkochen, Germany), is used for the test. Before the test, gold is sprayed on the surface of the sample to enhance the signal intensity. The element content of the hydration product was obtained by EDS surface scanning to analyze the element composition.

4. Results and Discussion

4.1. Determination of Optimal Mix Proportions

To ensure the reliability and comparability of the subsequent mechanical performance evaluation and micro-mechanism analysis, the optimal mix proportions of different alkali activator systems were first determined based on a control-variable approach. The 7-day unconfined compressive strength was adopted as the primary evaluation index, considering its strong correlation with early structural stability and engineering applicability

of solidified drilling cuttings. The test results of unconfined compressive strength under different mix proportions are presented in Figure 4.

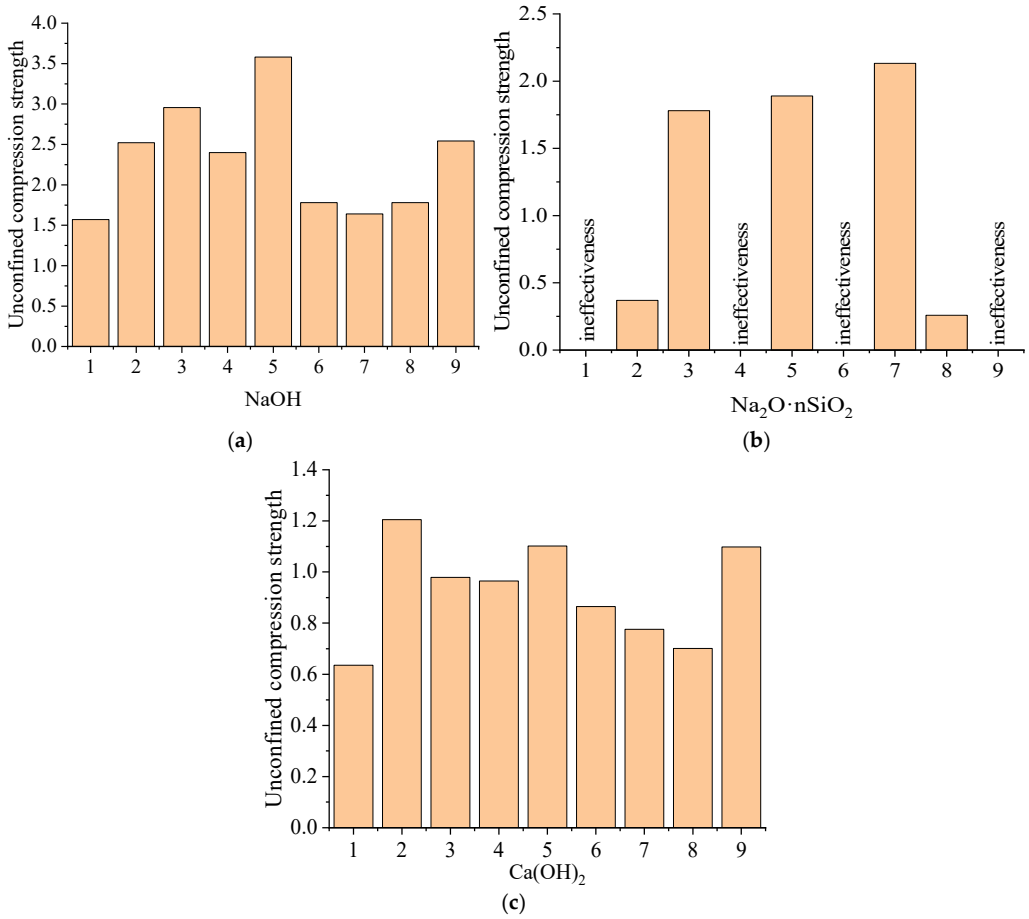

Figure 4. Unconfined compressive strength under different material mix proportions: (**a**) Sodium hydroxide system; (**b**) $Na_2O{\cdot}nSiO_2$ system; (**c**) calcium hydroxide system.

As shown in Figure 4a, the unconfined compressive strength of the NaOH system increased initially and then decreased with increasing activator dosage and furnace ash content. When the NaOH dosage reached 4 wt.% and the furnace ash content was 20 wt.%, the solidified body exhibited the highest strength, indicating that this proportion provided a sufficiently strong alkaline environment to promote the dissolution of active Si and Al phases and the formation of dense gel products. Excessive NaOH, however, led to marginal strength reduction, which may be attributed to the formation of micro-cracks caused by alkali over-reaction and increased porosity.

For the $Na_2O{\cdot}nSiO_2$ system (Figure 4b), the overall strength level was slightly lower than that of the NaOH system but still showed a clear dependence on mix proportion. The optimal performance was obtained at 3 wt.% activator dosage combined with 20 wt.% furnace ash. When the activator dosage exceeded this level, the strength gain became limited, possibly due to the imbalance between silica supply and calcium availability.

In contrast, the $Ca(OH)_2$ system (Figure 4c) demonstrated relatively lower unconfined compressive strength values and weaker sensitivity to proportion variation. The best performance was achieved at 4 wt.% $Ca(OH)_2$ and 15 wt.% furnace ash. Although $Ca(OH)_2$ could provide an alkaline environment, its activation efficiency was comparatively limited. Increasing furnace ash content beyond the optimal range did not further enhance strength.

Based on the above comparative analysis, the optimal mix proportions for subsequent experiments were determined as 4 wt.% NaOH + 20 wt.% furnace ash, 3 wt.% $Na_2O{\cdot}nSiO_2$ + 20 wt.% furnace ash, and 4 wt.% $Ca(OH)_2$ + 15 wt.% furnace ash, respectively.

4.2. Effect of Activator Type on the Compressive Strength of Solidified Drilling Cuttings

The compressive strength of the specimens under different activator types is shown in Figure 5. When the activator is NaOH, the 7-day compressive strength is 2.40 MPa, and the 28-day compressive strength is the highest, which is 4.81 MPa. When the activator is $Na_2O{\cdot}nSiO_2$, the 7-day compressive strength is 2.13 MPa, and the 28-day compressive strength is 3.21 MPa. When the activator is a Ca-based alkaline agent, the 7-day compressive strength is 1.21 MPa, and the 28-day compressive strength is 1.92 MPa. It can be seen from the data that the three kinds of solidified drilling cuttings all meet the requirements of the 'Highway Asphalt Pavement Design Specification' (JTG D50-2017) for the 7-day unconfined compressive strength of the base [18], but the type of activator has a significant effect on the curing, among which NaOH has the best strengthening effect, followed by $Na_2O{\cdot}nSiO_2$, and the Ca-based alkaline agent, which has the weakest effect. This observation is consistent with the findings of Fu et al. [16], who reported that appropriate regulation of the activator system can significantly enhance the mechanical properties of drilling-cuttings-based solidified materials. The strongly alkaline environment generated by NaOH (pH > 12.5) facilitates the dissolution of reactive Si and Al species in the ash, whereas $Ca(OH)_2$ only provides a moderately alkaline condition (pH ≈ 11.5–12.0), which is insufficient to effectively initiate polymerization reactions.

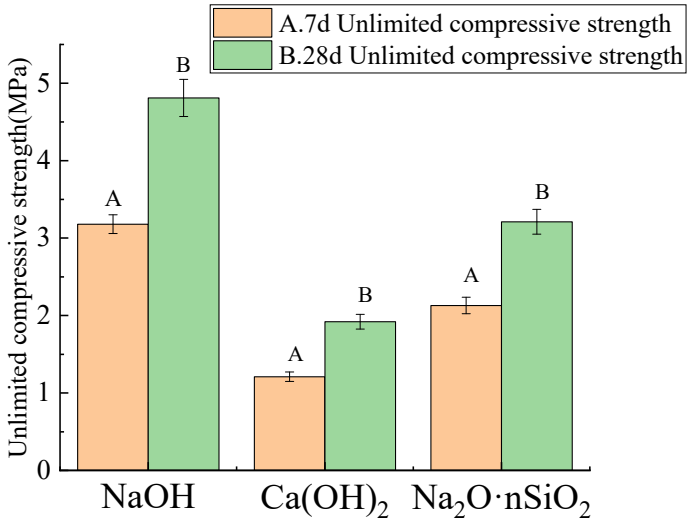

Figure 5. Compressive strength of drilling cuttings solidified by different activators.

With the increase in curing age, the compressive strength of the samples shows an upward trend, which is due to the continuous alkali activation reaction during the curing process, and the continuous accumulation of hydration products promotes the gradual densification of the sample structure. High strength and its early compressive strength help to broaden the application scenarios of solidified drilling cuttings [19].

4.3. Effect of Activator Type on Splitting Tensile Strength of Solidified Drilling Cuttings

The splitting tensile strength under different activator types is shown in Figure 6. It can be seen from Figure 6 that the splitting tensile strength under different activator types is significantly different. The splitting tensile strength of the NaOH system reaches 0.38 MPa at 7 days and rises to 0.41 MPa at 28 days. The strength of the $Na_2O{\cdot}nSiO_2$ system at 7 days and 28 days was 0.13 MPa and 0.22 MPa, respectively. The performance

of the Ca $(OH)_2$ system is the weakest; at 7 days, it is only 0.07 MPa, and at 28 days, it is 0.09 MPa. The regulatory effect of activator type on splitting tensile strength is distinct. NaOH has the best strengthening effect, followed by $Na_2O{\cdot}nSiO_2$, and $Ca(OH)_2$ has the weakest activation ability, which is consistent with the efficiency law of activator in the previous compressive strength test. With the extension of curing age, the splitting tensile strength of each sample showed an increasing trend, reflecting that the alkali-activated hydration reaction continued to advance during the curing process, and the accumulation of hydration products could enhance the interfacial bonding between the particles inside the sample.

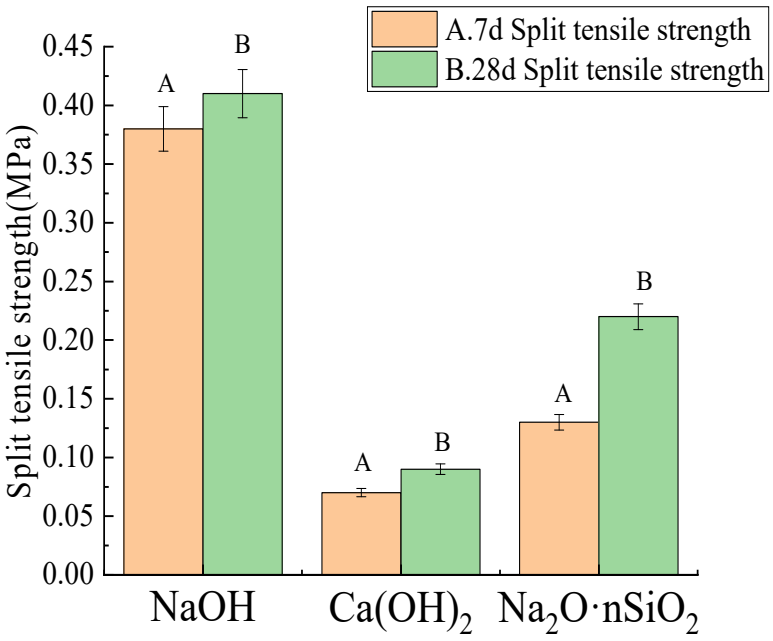

Figure 6. Splitting tensile strength of drilling cuttings solidified by different activators.

The mechanical properties test data clarify the regulation law of different activators on the mechanical properties of solidified drilling cuttings, and the mechanism of the microscopic characteristics, such as internal interface structure and hydration product morphology, on the splitting tensile properties needs to be further analyzed in combination with XRD, SEM, and other microscopic characterization methods.

4.4. Effect of Activator Type on Unconfined Compressive Strength of Cuttings in Solidified Drilling After Dry–Wet Cycles

The evolution of the unconfined compressive strength of the solidified body with the number of dry–wet cycles under different activator types is shown in Figure 7. The three curves showed a significant downward trend, indicating that with the increase in the number of dry–wet cycles, the unconfined compressive strength of the solidified bodies of the three alkali-activated systems showed continuous attenuation characteristics, revealing that the dry–wet cycle would accelerate the damage of the internal structure of the material, which in turn led to the deterioration of its mechanical properties. The results of the dry–wet cycle test further show that the durability of the solidified bodies of the three alkali-activated systems is closely related to their initial strength and microstructure. In the NaOH system, the initial strength is the highest, close to 4.7 MPa, and the highest strength of the three is always maintained at all cycles. At the ninth cycle, it is still maintained at about 3.4 MPa, and the strength retention rate is about 7. The high strength retention rate (≈73%) of the NaOH system is consistent with the discovery of Song et al. [15] that the

dense gel structure can effectively resist water erosion, which is also the key basis for the system to have engineering application potential. This confirms that the microstructure composed of dense C-(N)-A-S-H and C-S-H gels can effectively delay the damage caused by water erosion. In the $Na_2O{\cdot}nSiO_2$ system, the initial strength is about 3.1 MPa, the strength level is always in the middle, and it drops to about 2.3 MPa at the ninth cycle. The strength retention rate is about 74%. In the Ca $(OH)_2$ system, the initial strength is the lowest, about 1.7 MPa, and the whole strength is the lowest. At the ninth cycle, it is only about 1.2 MPa, and the strength retention rate is about 71%. It is attributed to its loose structure dominated by plate-like crystals and lack of gelling gel, which cannot resist the stress caused by dry–wet alternation. Under the condition of dry–wet cycle, the type of activator determines the durability of the solidified body by affecting the composition and pore structure of the gelled product. The NaOH excitation system has the best performance in maintaining a high strength retention rate, and has the potential to be used in engineering conditions that require durability; however, due to the serious lack of durability, the application scenarios of Ca $(OH)_2$ system will be greatly limited.

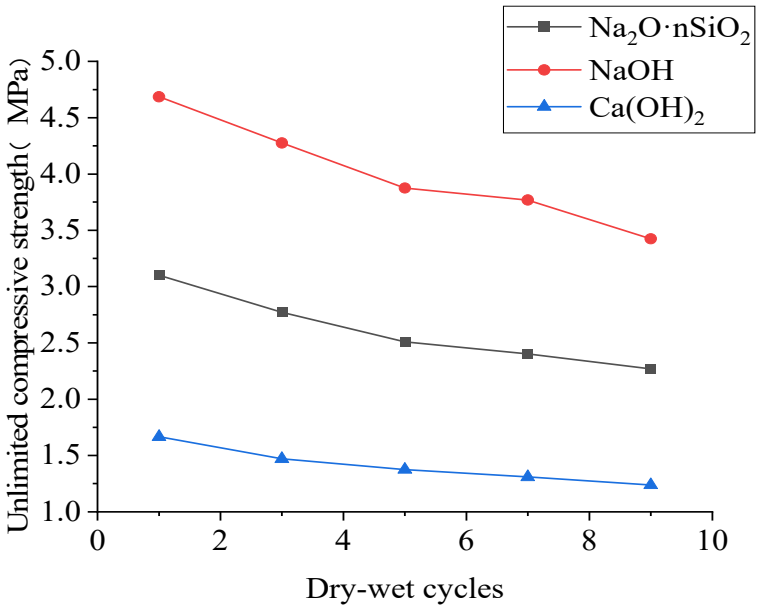

Figure 7. Unconfined compressive strength after dry–wet cycle under different activators.

4.5. XRD Analysis

The XRD patterns of drilling cuttings after standard curing for 7 days and 28 days under different activator types are shown in Figure 8. It can be seen from Figure 8 that the XRD patterns of all samples retain obvious SiO_2 characteristic peaks, indicating that even in an alkaline environment, only a small amount of quartz cannot participate in the geo polymerization reaction. The hydrated gel generated by alkali activation in drilling cuttings mainly exists in an amorphous state. Among them, the broad dispersion peaks in the diffraction angle range of 25°~35° corresponded to gel phases such as C-(N)-A-S-H and C-S-H. The wide scattering peak of NaOH system at 25°~35° is consistent with the research results of Gao et al. [9]. It is shown that the C-A-S-H gel formed by alkali-activated reaction has pore filling and chemical cementation, which is the core of improving the mechanical properties of the substrate. Under the high alkaline environment (pH > 12) excited by NaOH, the participation of Na^+ promotes the polymerization of active Si/Al components to form N-A-S-H, which is combined with trace Ca^{2+} in the system to convert into C-(N)-A-S-H. When excited by $Na_2O{\cdot}nSiO_2$, the additional SiO_3^{2-} further promoted the accumulation of such gel phase. However, the alkalinity of the Ca-based alkaline

agent system is weak (pH < 12), and the reaction kinetics between Ca^{2+} and active Si/Al in drilling cuttings are insufficient. The intensity of the dispersion peak in this region is significantly weak, and the corresponding C-A-S-H gel production is limited [19].

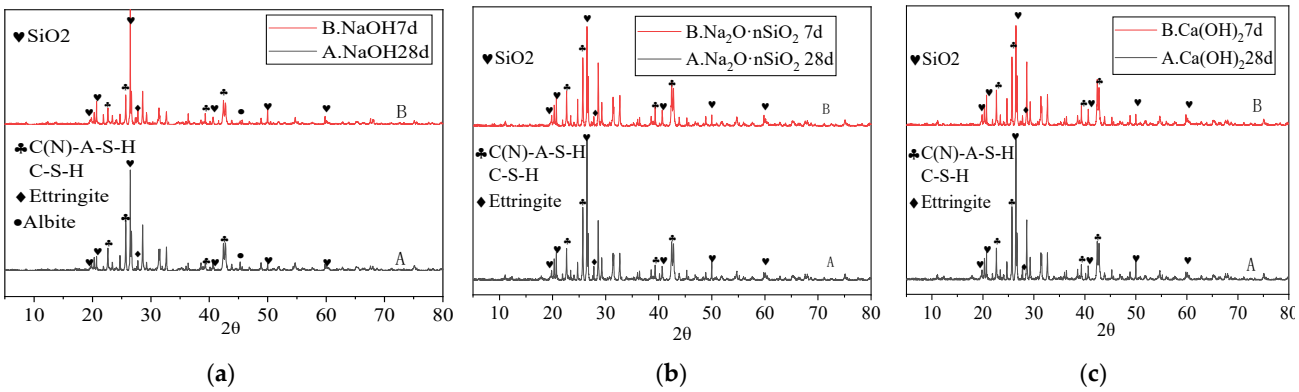

Figure 8. XRD patterns: (**a**) Sodium hydroxide system; (**b**) $Na_2O{\cdot}nSiO_2$ system; (**c**) calcium hydroxide system.

Compared with the NaOH system, the dispersion peak intensity of the C-(N)-A-S-H/C-S-H gel in the 25°–35° range of the XRD spectrum (Figure 8c) is significantly weaker due to the lack of alkalinity of the calcium-based alkaline regulator, which confirms that it cannot fully activate the active component and can only generate a small amount of gel through a slow pozzolanic reaction.

The filling and cementation of such an amorphous gel is the core support for improving the compactness and mechanical properties of alkali-activated furnace ash solidified drilling cuttings. Among them, when NaOH and $Na_2O{\cdot}nSiO_2$ are used as activators, the gel contribution of the solidified material is more prominent, while under the action of $Ca(OH)_2$, the gel effect is relatively weak. Because the diffraction peaks of C-(N)-A-S-H and C-S-H are partially overlapped, and both of them show amorphous dispersion characteristics, it is difficult to identify the main peaks of these two types of products by XRD alone.

4.6. Laser Particle Size Analysis

The laser particle size analysis curves under different activator types are shown in Figure 9. It can be seen from Figure 9 that the proportion of fine particles in solidified drilling cuttings is in the order of 'NaOH > $Na_2O{\cdot}nSiO_2$ >$Ca(OH)_2$': the proportion of fine particles in NaOH system is high, and its bulk density is 1~10 μm as the main peak (bulk density > 3%), and the cumulative distribution at 10 μm accounts for more than 70%. The proportion of fine particles in the $Na_2O{\cdot}nSiO_2$ system is medium, and the peak volume density is also located in the range of 1–10 μm, but the height is less than 2.5%. The particle distribution is slightly dispersed, and the cumulative proportion at 10 μm is about 60%. The proportion of fine particles in the $Ca(OH)_2$ system is low, the peak volume density moves to the range of 10~100 μm (peak < 1.5%), the particle distribution range is wide (0.1~1000 μm), and the cumulative proportion at 10 μm is less than 40%. The fine particles (1~10 μm) of the solidified body of the NaOH system accounted for more than 70%, and the particle distribution was concentrated. Combined with the results of the dry–wet cycle test (nine cycles of strength retention rate ≈ 73%), its compactness and water resistance were better; the coarse particles (10–100 μm) of $Ca(OH)_2$ system account for a high proportion and are dispersed. The corresponding dry–wet cycle strength retention rate is only 71%, and the compactness and durability are poor. This rule is mutually confirmed with the results of laser particle size analysis [20].

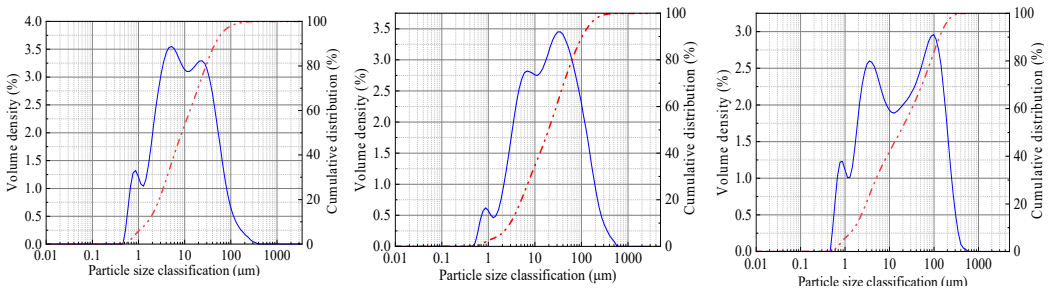

Figure 9. Laser particle size analysis curves: (**a**) Sodium hydroxide system; (**b**) $Na_2O{\cdot}nSiO_2$ system; (**c**) calcium hydroxide system.

4.7. TG-DSC Analysis

The synchronous thermal analysis curves of different curing systems after 28 days of standard curing are shown in Figure 10. It can be seen from the figure that the mass loss of the drilling cuttings alkali excitation formula can be roughly divided into three stages: the first stage is 0~150 °C, and the mass loss in this interval is mainly due to the decomposition of free water, physically adsorbed water and weakly bound water in the system. The weight loss of $Ca(OH)_2$ system was 14.20%, $Na_2O{\cdot}nSiO_2$ system was 10.34%, and NaOH system was only 9.99%, which was related to the denser structure and lower free water adsorption capacity of the latter product. The temperature of the second stage is 150~500 °C, and the weight loss in this stage corresponds to the dehydroxylation of the stable bound water in the gel, accompanied by the decomposition of a small amount of organic matter in the cuttings. It is worth noting that in the range of 400–450 °C, the TG curve of the $Ca(OH)_2$ system exhibits a characteristic weight loss step, and an endothermic peak appears on the DSC curve. This is attributed to the dehydration decomposition of free $Ca(OH)_2$ ($Ca(OH)_2 \rightarrow CaO + H_2O$), which is not involved in the reaction. Based on the characteristic weight loss of the $Ca(OH)_2$ phase at 400–450 °C (1.65%) and the theoretical weight loss ratio of $Ca(OH)_2$ dehydration (24.3%), the content of free $Ca(OH)_2$ in the solidified matrix was calculated to be approximately 6.8%. The calculation results are consistent with the morphology of a large number of hexagonal plate-like $Ca(OH)_2$ crystals clearly visible in SEM observation (Figure 11e,f), indicating that under weakly alkaline excitation conditions, the calcium source fails to fully participate in the pozzolanic reaction and mostly exists in an unreacted crystalline form, resulting in insufficient cementation products. The temperature of the third stage is 500~800 °C, and the weight loss in this interval is mainly related to the thermal decomposition of carbonate. The weight loss (9.6%) and thermal effect of $Ca(OH)_2$ system are the most obvious [21].

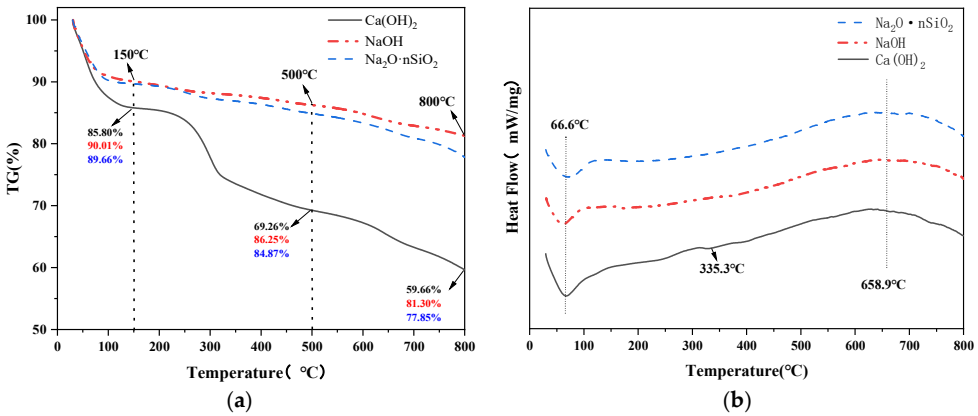

Figure 10. Synchronous thermal analysis curves: (**a**) TG curve; (**b**) DSC curve.

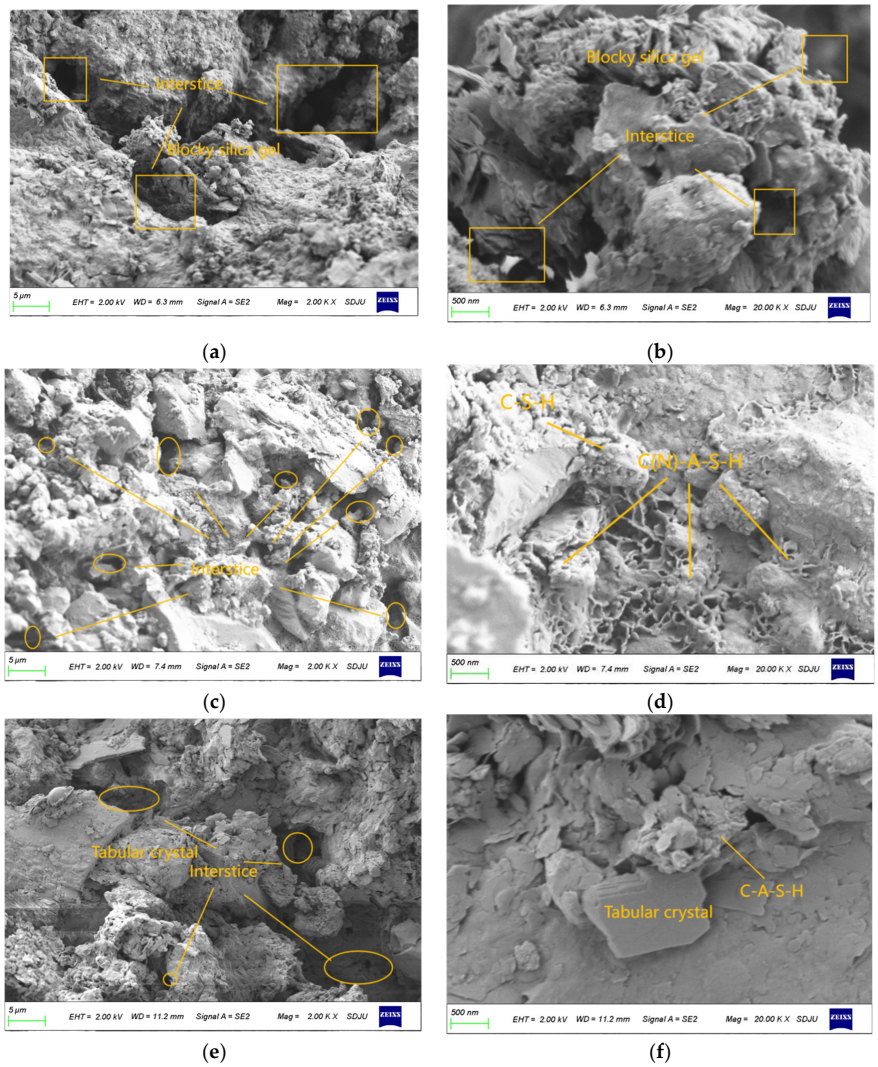

Figure 11. Microscopic morphology of solidified drilling cuttings under different activators: (**a**) $Na_2O{\cdot}nSiO_2$ 2 KX; (**b**) $Na_2O{\cdot}nSiO_2$ 20 KX; (**c**) sodium hydroxide 2 KX; (**d**) sodium hydroxide 20 KX; (**e**) calcium hydroxide 2 KX; (**f**) calcium hydroxide 20 KX.

From the DSC curve, it can be seen that within 150 °C, the endothermic peak near 66.6 °C corresponds to the water phase evaporation process in the range of 0~150 °C. The endothermic peak enthalpy of the $Ca(OH)_2$ system (133.5 J/g) is significantly higher than that of the NaOH system (78.3 J/g). The endothermic peak at about 335.3 °C corresponded to the dehydroxylation of bound water and the decomposition of organic matter in the range of 150–500 °C, and only showed an obvious peak shape under the activation of $Ca(OH)_2$. The exothermic peak near 658.9 °C corresponds to the decomposition of carbonate in the range of 500~800 °C, and the peak intensity of the $Ca(OH)_2$ system is also the most prominent.

Combined with XRD and other microscopic test results, it can be seen that the hydration products of the drilling cuttings alkali activation system are mainly C-S-H and C-(N)-A-S-H gels. The difference in the effect of different activators is directly reflected in the degree of weight loss and peak shape characteristics of thermal behavior.

4.8. SEM-EDS Analysis

The microstructure of solidified drilling cuttings after 28-day hydration under different types of alkali activators is presented in Figure 11. It can be observed that all specimens contain voids, gel phases, and pores post-hydration. When $Na_2O{\cdot}nSiO_2$ is used as the alkali

activator, the low-magnification image reveals numerous long, strip-shaped open pores; these pores are interconnected and large in size. At high magnification, massive silica gel is only distributed in local regions, while most particle interfaces remain distinct with no cementitious material present. This indicates that the activation efficiency of $Na_2O{\cdot}nSiO_2$ for drilling cuttings is low, and the distribution of hydration products is uneven. For the NaOH system, the low-magnification image shows a densely packed overall structure, with pores mostly existing as closed, small-sized ones. At high magnification, C(N)-A-S-H gel and flocculent C-S-H are interwoven and have filled the particle gaps. The synergistic effect of these two gels forms the skeletal strength, which corresponds to the result that the unconfined compressive strength of the NaOH-activated specimen is the highest among all tested combinations. The highly reactive hydration products generated under NaOH activation fully exert their cementitious role. In the low-magnification image of the $Ca(OH)_2$ system, the pores are coarse in size and highly interconnected. At high magnification, a large number of hexagonal plate-like $Ca(OH)_2$ crystals (with sharp edges and corners) are distributed independently, while gel products (e.g., C-S-H) are scarce. This is attributed to the insufficient alkalinity of $Ca(OH)_2$, which fails to effectively activate the reactivity of furnace ash—ultimately leading to a loose structure and decreased mechanical strength.

The energy spectrum and EDS analysis results of 28-day solidified drilling cuttings under different activators are presented in Figure 12. It should be noted that the carbon(C) signal detected in the EDS analysis may be partially attributed to residual carbon tape from the sample preparation process; however, this contamination does not interfere with the assessment of the distribution trends of major elements including Ca, Si, and O. The EDS surface scanning results of NaOH-treated samples show that the distribution of Ca (15.8%) and Si (4.2%) elements is highly overlapped and is consistent with the distribution area of O element, indicating that the Ca and Si components react extensively in this excitation environment. Although rod-like and amorphous morphologies are observed in the SEM micrographs, the typical slender needle-like crystalline features characteristic of ettringite (AFt) are absent. More importantly, no characteristic diffraction peaks corresponding to AFt are detected in the XRD patterns. By integrating these two key lines of evidence—the absence of AFt characteristic peaks in XRD and the lack of its typical needle-like morphologies in SEM—the formation of a substantial amount of AFt can be conclusively ruled out. The measured Ca/Si atomic ratio is about 3.6. Combined with its microscopic morphology, it is speculated that the main hydration products may be C-S-H gels with a high calcium–silicon ratio or other calcium-rich silicate phases. This dense reaction product structure is consistent with its highest unconfined compressive strength. It is worth noting that no distinct Al signal was detected via EDS surface scanning, which can be attributed to two primary factors. First, the Al-Kα peak (~1.49 keV) partially overlaps with the Si-Lα peak (~1.74 keV) in the energy spectrum, particularly at low elemental contents. Second, carbon contamination potentially introduced by carbon tape further interferes with the accurate detection of elements in the low-energy region. Nevertheless, the broad diffused peaks in the 25°–35° range of the XRD pattern (Figure 7) are clearly attributable to the C-(N)-A-S-H gel phase, where 'A' denotes aluminum (Al) incorporated into the gel network. This directly confirms that Al participated in the alkali-activation reaction and was incorporated into the gel structure during the reaction process. For the $Na_2O{\cdot}nSiO_2$-treated samples, the Ca content is 9.1%, and the Si content is 2.9%; Si is locally enriched, while Ca is dispersed. The Ca-Si reaction activity is low, so only a small amount of silica gel is formed; most of the Ca exists in a free state and cannot contribute to effective cementation. For the $Ca(OH)_2$-treated samples, the Ca content is 17.5%, and the Si content is 4.2%. Ca agglomerates (corresponding to the hexagonal plate-like crystals observed via SEM) are present, while the distribution of Si and O is sparse. Owing to insufficient active

silica, Ca exists only in crystalline form, with no gel-type cementitious products present. In summary, the type of alkali activator dictates the type and cementation efficiency of hydration products by regulating the content and spatial distribution of Ca and Si; this, in turn, governs the macroscopic mechanical properties of the alkali-activated drilling cuttings solidified body.

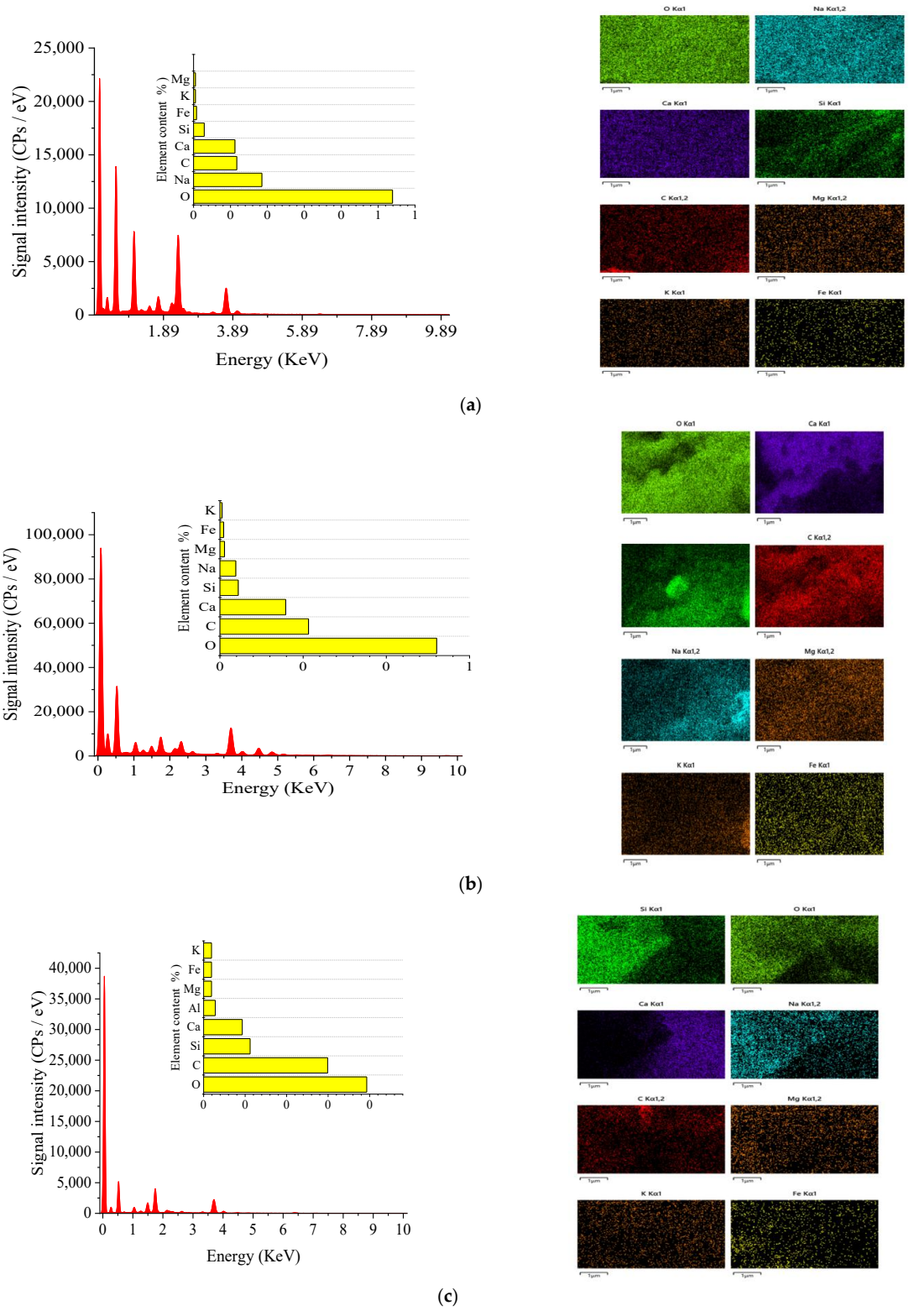

Figure 12. EDS images of drilling cuttings solidified by different activators: (**a**) $Na_2O{\cdot}nSiO_2$ system; (**b**) sodium hydroxide system; (**c**) calcium hydroxide system.

5. Conclusions

In this study, three alkali activators (NaOH, $Na_2O{\cdot}nSiO_2$, and $Ca(OH)_2$) were employed to activate furnace ash for the solidification of oilfield drilling cuttings, and the mechanical performance, durability, and microstructural characteristics of the resulting solidified materials were comparatively investigated. The major conclusions are summarized as follows:

(1) The optimal mix proportions were determined based on the 7-day unconfined compressive strength. The recommended ratios were 4 wt.% NaOH + 20 wt.% furnace ash for the NaOH system, 3 wt.% $Na_2O{\cdot}nSiO_2$ + 20 wt.% furnace ash for the $Na_2O{\cdot}nSiO_2$ system, and 4 wt.% $Ca(OH)_2$ + 15 wt.% furnace ash for the $Ca(OH)_2$ system.

(2) The type of alkali activator has a decisive influence on the strength performance of the solidified drilling cuttings. Among the three systems, the NaOH-activated specimens exhibited the highest compressive strength, followed by the $Na_2O{\cdot}nSiO_2$ system, while the $Ca(OH)_2$ system showed comparatively lower strength. Nevertheless, all three systems satisfied the 7-day unconfined compressive strength requirements specified in the Highway Asphalt Pavement Design Specification (JTG D50-2017), indicating the feasibility of synergistic utilization of drilling cuttings and furnace ash in road engineering applications.

(3) The performance differences among the three systems are primarily attributed to variations in gel formation and structural compactness induced by different activators. The NaOH system produced a denser and more stable microstructure, which contributed to superior mechanical strength and durability, whereas the $Ca(OH)_2$ system formed a relatively loose structure with weaker long-term stability.

(4) From an engineering and economic perspective, although the material cost of the NaOH-based system is higher than that of $Ca(OH)_2$, it demonstrates significantly enhanced strength and durability while remaining more economical than the $Na_2O{\cdot}nSiO_2$ system. The optimized mix proportion (4 wt.% NaOH + 20 wt.% furnace ash) achieves a balanced performance–cost ratio, making it more suitable for oilfield road base applications where strength and durability requirements.

Additional notes: Comparison of industrial-grade unit costs of three alkaline adjustment materials are as follows: $Ca(OH)_2$ (about 1200~1500 yuan/ton) < NaOH (about 3000~3500 yuan/ton) < $Na_2O{\cdot}nSiO_2$ (water glass, modulus 2.23, about 4000~4500 yuan/ton). Although the cost of the 4% NaOH + 20% furnace ash system determined in this study is higher than that of the $Ca(OH)_2$ system, the mechanical properties and durability are significantly better (the 28-day compressive strength is increased by more than 150%), and the cost is lower than that of the $Na_2O{\cdot}nSiO_2$ system. The 'performance–cost' balance is achieved, which is more suitable for engineering scenarios such as oilfield road bases with clear requirements on strength.

6. Future Research Perspectives

This study evaluated only three representative single alkaline activators, namely NaOH, $Ca(OH)_2$, and $Na_2O{\cdot}nSiO_2$. The conclusions were derived from the synergistic reaction characteristics between drilling cuttings and coal-fired furnace ash obtained from the Maye Oilfield in Xinjiang. Due to the regional specificity of raw materials, the applicability of the findings may be limited to solid wastes with similar physicochemical and mineralogical properties. In practical cross-regional applications, the type and dosage of the activator, as well as the proportion of furnace ash, should be adjusted according to the chemical composition of the target solid waste, such as the active Si/Al ratio, organic matter content, and salinity. Furthermore, the adaptability of the proposed curing system to drilling cuttings with more complex characteristics still requires further verification.

In addition, this study primarily focused on single-alkali-activator systems and did not systematically investigate the synergistic effects of composite activators, such as the combination of NaOH and sodium silicate. Future research will therefore explore composite activation systems and optimize compounding ratios to achieve a better balance between mechanical performance and economic cost, thereby improving the engineering applicability and universality of the curing system.

Author Contributions: Conceptualization, A.Q., W.H. and Y.L.; Methodology, W.L.; Software (use of data processing tools), Y.Z.; Validation, P.W., Y.Z. and Z.W.; Formal Analysis, A.Q. and Y.Z.; Investigation, A.Q. and P.W.; Resources (coordination of experimental materials/equipment), Z.W.; Data Curation, A.Q. and J.J.; Writing—Original Draft Preparation, A.Q. and J.J.; Writing—Review and Editing, W.H., Y.L. and W.L.; Visualization (creation of figures and tables), Y.Z.; Project Administration, W.H. and Y.L.; Funding Acquisition, W.H. and Y.L. All authors have read and agreed to the published version of the manuscript.

Funding: This work was supported by the National Natural Science Foundation of China (Grant No. 52508507), project entitled "Study on controlled synthesis of crumb rubber/CNTs cross-scale reinforcement modified asphalt based on induced polymerization technology and multi-scale interface interaction mechanism".

Institutional Review Board Statement: Not applicable.

Informed Consent Statement: Not applicable.

Data Availability Statement: The original contributions presented in this study are included in the article. Further inquiries can be directed to the corresponding authors.

Conflicts of Interest: Achen Qi, Pei Wang, Yuanjie Zhu, Wei Liu were employed by the Heavy Oil Development Company of PetroChina Xinjiang Oilfield Company. The remaining authors declare that the research was conducted in the absence of any commercial or financial relationships that could be construed as a potential conflict of interest.

Abbreviations

The following abbreviations are used in this manuscript:

XRD	X-Ray Diffraction
SEM	Scanning Electron Microscopy
EDS	Energy Dispersive Spectrometer
TG	Thermal Gravimetric Analyzer
DSC	Differential Scanning Calorimetry

References

1. Li, J.; Chen, D.B.; Yu, Q.J.; Yin, S.H. Reaction Process of Slag in Sodium Hydroxide Solutions with Different Concentrations. *J. Chin. Ceram. Soc.* **2024**, *52*, 1508–1519. [CrossRef]
2. Sun, X.; Liu, J.; Qiu, J.; Ren, H.; Liu, C.; Li, X.; Li, Z. Alkali activation of blast furnace slag using a carbonate-calcium carbide residue alkaline mixture to prepare cemented paste backfill. *Constr. Build. Mater.* **2022**, *320*, 126234. [CrossRef]
3. Mounika, G.; Ramakrishna, U.; Reddy, G.N.K.; Kumar, K.S. A review on effect of red mud on properties of alkali activated materials (AAMs) and geopolymers (GPs). *Mater. Today Proc.* **2023**, *3*, S221478532301492X. [CrossRef]
4. Wang, C. Study on the Properties of Alkali-Activated Cementitious Materials. Master's Thesis, Harbin Institute of Technology, Harbin, China, 2006; p. 5.
5. Liu, X.; Wan, M.Y.; Shi, G.D.; Xu, R.S.; Li, C.L.; Jiang, T.; Xuan, W.Z. Preparation and Mechanical Properties of Alkali-Activated Geopolymer Cementitious Materials Modified with Lignocellulose. *Metal Mine* **2024**, *8*, 252–258.
6. Wang, Y.F.; Lei, L.; Shi, C.J. Effect of diethanolisopropanolamine and ethyldiisopropylamine on hydration and strength development of cement-fly ash-limestone ternary blend. *Cem. Concr. Compos.* **2024**, *145*, 105354. [CrossRef]
7. Tu, W.L.; Fang, G.H.; Dong, B.Q.; Zhang, M.Z. Multiscale study of microstructural evolution in alkali-activated fly ash-slag paste at elevated temperatures. *Cem. Concr. Compos.* **2023**, *143*, 105258. [CrossRef]

8. Zhang, L.; Wen, P.H.; Wang, C.H.; Geng, S.G.; Di, W.Y. Research Progress on Trenchless Grouting Reinforcement and Repair Materials for Roads. *Mater. Rev.* **2017**, *31*, 98–105.
9. Gao, Y.L.; Chen, T.F.; Li, Y.L.; Li, W.G. Performance and Microscopic Characteristics of All-Solid Waste Alkali-Activated Cementitious Material Stabilized Soil. *J. Changsha Univ. Sci. Technol.* **2025**, *22*, 1–10. [CrossRef]
10. Jing, Y.H.; Zhang, Y.N.; Wang, Q.J.; Shang, Y.Z.; Zhang, L. Study on the hydration characteristics of alkali-activated spontaneous combustion coal gangue-based cementitious materials. *J. Liaoning Tech. Univ. (Nat. Sci.)* **2025**, *44*, 659–666.
11. Li, D.; Zheng, W.; Wang, Y. Preparation and properties of alkali-activated slag-like powder paste. *J. Mater. Res. Technol.* **2025**, *35*, 611–627. [CrossRef]
12. Li, Y.G.; Yang, H.J.; Mei, H.; Wang, Y. Study on Structural Characteristics and Function of XSG Curing Agent for Waste Drilling Fluid. *Xinjiang Pet. Gas* **2012**, *8*, 101–104.
13. Yang, H.J.; Mei, H.; Hu, Y.G.; Li, Y.G. Laboratory Experimental Evaluation on the Composition of XSG Curing Agent for Waste Drilling Fluid. *Xinjiang Pet. Gas* **2011**, *7*, 76–81.
14. Han, B.; Cai, L.; Chi, F.; Zhan, W. Impact of metakaolin to partially replace granulated blast furnace slag on the performance of alkali-activated slag grouting materials and evaluation of grouting effectiveness. *Mater. Res. Express* **2025**, *12*, 025507. [CrossRef]
15. Song, Y.Z.; Zhao, Q.L.; Yao, X.J.; Ma, W.J. Silicon Source Regulation of Steel Slag-Based Alkali-Activated Cementitious Materials and Its Strength Evolution Mechanism. *Bull. Chin. Ceram. Soc.* **2025**, *44*, 3705–3712. [CrossRef]
16. Fu, J.X.; Chen, G.; Wang, Q. Analysis of Reaction Mechanism and Mechanical Properties of Alkali-Activated Slag Solidified Peaty Soil. *Chin. J. Geotech. Eng.* **2021**, *43*, 1871–1878.
17. *JTG 3441-2024*; Ministry of Transport of the People's Republic of China. Test Methods of Materials Stabilized with Inorganic Binders for Highway Engineering. China Communications Press Co., Ltd.: Beijing, China, 2024.
18. *JTG D50-2017*; Ministry of Transport of the People's Republic of China. Specifications for Design of Highway Asphalt Pavement. China Communications Press Co., Ltd.: Beijing, China, 2017.
19. Hu, Z.H.; Gu, X.W.; Li, Z.J.; Wang, H.; Liu, Y. A novel solid waste activator for coal gasification slag-based geopolymers: Sodium-based desulfurization ash and carbide slag. *Constr. Build. Mater.* **2025**, *470*, 140655. [CrossRef]
20. Cao, R.L.; Jia, Z.J.; Zhang, S.Q.; Liu, J.; Wu, Y.X.; Chen, G.N. Effect of low-calcium and high-magnesium ferronickel slag on the microstructure and micromechanical properties of alkali-activated blended ground granulated blast furnace slag. *Constr. Build. Mater.* **2023**, *406*, 133421. [CrossRef]
21. Grant Norton, M.; Provis, J.L. 1000 at 1000: Geopolymer technology—The current state of the art. *J. Mater. Sci.* **2020**, *55*, 13487–13489. [CrossRef]